ARTICLE IN PRESS

Synthetic Metals xxx (xxxx) xxx

Contents lists available at ScienceDirect

Synthetic Metals

journal homepage: www.elsevier.com/locate/synmet

Research paper

Electromagnetic wave absorption characteristics of single and double layer absorbers based on trimetallic FeCoNi@C metal−organic framework incorporated with MWCNTs

Omid Mirzaee [a], Isabelle Huynen [b,*], Mohsen Zareinejad [c]

[a] Faculty of Materials and Metallurgical Engineering, Semnan University, P.O. Box 35196-363, Semnan, Iran
[b] ICTEAM Institute, ELEN Division, Place du Levant 3, Louvain-la-Neuve B-1348, Belgium
[c] Young Researchers and Elite Club, Shiraz Branch, Islamic Azad University, Shiraz, Iran

A R T I C L E I N F O

Keywords:
Metal−organic framework
MWCNTs
Single and double-layer
Electromagnetic properties
Microwave absorption

A B S T R A C T

The present study focuses on the design of single and double layer microwave absorbers based on FeCoNi@C metal−organic framework incorporated with MWCNTs. FeCoNi@C metal−organic framework (MOF) and MWCNTs decorated with MOF (MW/MOF) were successfully synthesized via hydrothermal method and characterized with XRD, VSM and FESEM. The electromagnetic parameters of material (complex permittivity and permeability) of the as-prepared nanocomposites dispersing in paraffin (30 wt% powder, single layer) were evaluated by a vector network analyzer in X-band frequency range. The simulation of microwave absorption performance of single- and double-layer absorbers was performed via CST Studio software. The results indicate that the double layer absorber using M/MOF structure as matching layer and MOF structure as absorbing layer can increase the microwave absorption bandwidth up to 4 GHz and greatly decrease the reflection loss down to −36 dB for a total thickness of 2 mm. In contrast, the single layer microwave absorber consisting of 30 wt% M/MOF composite structure exhibited a minimum reflection loss of −18 dB at 9 GHz with 2 GHz bandwidth and 2.5 mm thickness. The better absorption performance of the double-layer absorber maybe attributed to the better impedance matching ability of M/MOF layer, coupling interactions between two distinctive layers (absorbing and matching layers) and excellent magnetic loss ability of MOF layer.

1. Introduction

With the ever growing increase of communications systems, there is a crucial need for compact lightweight devices combining compactness and reliability. The constraints are antagonist if we consider that reduced size increases the risk of harmful electromagnetic interferences between electronic components. The same risk occurs from the wireless propagation which may be detrimental to both electronic devices and human body [1]. Therefore, since more than one decade, research is conducted on efficient microwave absorbing structures (MAS) aiming at blocking such interferences. Among these, polymer composites combining conductive carbon nanotubes and polymer hosting matrix offer several advantages; high conductivity at low loading rate owing to very good dispersion, mechanical stiffness as well as possibility of conformability for stealth application, lightweight as compared to metallic shields, etc. Compared to other filling charges such as carbon black particles CNT achieve a given level of conductivity at a much lower concentration, due to their very high aspect ratio favoring contact in between, hence the formation of a conducting percolation network at very low concentration, and finally an excellent level of absorption [2]. MAS can be designed to reduce the radar cross-section (RCS) of various objects for military as well civil applications: an absorbing shield covering the target is used to reduce by absorption the signal reflected by the target towards the radar, making the target almost invisible to radar (concept of stealth). Well-known applications of this are military airplanes (stealth bombers) and towers of wind farms, that need to be stealth for security reasons, i.e., to ensure invisibility or avoid spurious signatures perturbing the control of the traffic in civil air traffic. A dedicated family of absorbers is developed to reduce the RCS: the Salisbury screen configuration [3,4], based on an absorbing layer covering the target is assumed to be metallic, is thus reflective. The conductivity of the layer and its thickness can be tuned in order to match the

* Corresponding author.
E-mail address: isabelle.huynen@uclouvain.be (I. Huynen).

https://doi.org/10.1016/j.synthmet.2020.116634
Received 15 September 2020; Received in revised form 8 November 2020; Accepted 12 November 2020

Please cite this article as: Omid Mirzaee, *Synthetic Metals*, https://doi.org/10.1016/j.synthmet.2020.116634

frequency and bandwidth of the absorption, depending on the applications. A well-known case is radar communications at X band (8–12.4 GHz) [5]. In [6,7], various MAS are studied, where carbon fillers, including carbon black, incorporated at different concentration levels in single as well as multilayer configurations, induce reflection below −10 dB. A good absorber aims at minimizing the reflection of a signal incident to its surface, while maximizing the absorption through its thickness. Conductive composites are suited to attenuate the signal, however conductive charges may also increase the reflection as do metallic shields. An adequate strategy in order to counterbalance this effect consists in incorporating magnetic charges into the composite [8–11]. This combination allows to decrease the equivalent impedance at input interface as close as possible to that of air. The reflection is consequently reduced and absorption favored via the penetration of the signal in the absorber. This approach was developed in [12] where Zn metal−organic frameworks (MOFs) were combined with reduced graphene oxide and porous nanocarbon in order to achieve reflection as low as −50.5 GHz at 14 GHz. In [13] the rational construction of one-dimensional core–shell nanowires is reported, utilizing a solution growth process for zeolitic imidazolate frameworks (ZIFs) shell on Ag nanowires and a temperature-controlled pyrolysis process; it allows the obtention of MAS with a highly intense narrowband microwave resonance. In [14] authors used multi walled carbon nanotubes (MWCNTs) as templates for growth of Co-based zeolitic imidazolate frameworks (ZIFs) and obtained a Co–C/MWCNTs composite by post pyrolysis, showing a minimum reflection loss (RL) of − 48.9 dB at 10 GHz. Authors in [15] report a controllable growth of polypyrrole (PPy) nanofibers in the nanochannels of MOFs to construct a now kind of nanocomposites. The formed PPy/ZIFs nanocomposites show a highly tunable electrical conductivity as well as a tunable electromagnetic absorption (EMA) property. The maximal frequency width with absorbing higher than 90% of incident electromagnetic waves reaches 7.24 GHz. Finally in [16], a chain-like PPy aerogel decorated with MOF-derived nanoporous Co/C (Co/C@PPy) was prepared by a self-assembled polymerization method. With a filler loading ratio of 10 wt%, the composite of Co/C@PPy achieves an optimal reflection loss value of - 44.76 dB, and the effective bandwidth (reflection loss lower than −10 dB) is as large as 6.56 GHz.

On the other hand Multilayer configurations of PNCs containing a single type of inclusion such as micrometric graphite and CNFs (single- and multi-wall nanotubes or nanofibers) designed with the help of optimization algorithms are also used to minimize EM absorption from 2 to 18 GHz and at various incident angles with a tradeoff in absorber thickness [17–19]. As further optimization, stepped-gradient concentrations in conductive inclusions is used to optimize the lowest possible reflection, hence maximizing absorption [20].

Our paper exploits this dual strategy. Indeed, we propose a microwave absorber based on composite materials combining carbon nanotubes (CNT) and FeNi magnetic particles (MNP). We have chosen metal organic framework materials and MWCNTs for decreasing the density of the absorber since both of these types of materials has intrinsically porous structure with low density. Also, according to their porous structure more losses are expected due to multiple reflections occurring on walls of the pores. Two composites are prepared and then combined numerically to for bilayer structures forming the first step of a gradient configuration, with the objective to decrease return loss associated to RCS and therefore increase the absorption through the samples. Section 2 details the synthesis procedure of MNP and CNT@MNP, as well as morphological and microwave characterization tools. Section 3 provides the structural/morphological analysis as well as the demonstration of the absorption performances of our composite through measurements of electromagnetic parameters and resulting minimal reflection losses observed in our structures. It also provides a comparison of performances of between monolayer and bilayer absorbers, while Section 4 concludes about our work.

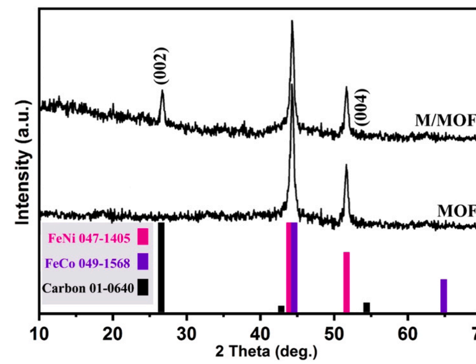

Fig. 1. X-ray diffraction patterns of MOF and M/MOF samples.

2. Experimental section

In the present study, iron chloride tetrahydrate, nickel nitrate hexahydrate, cobalt nitrate hexahydrate, N, N-dimethylformamide (DMF), 2,5-dihydroxyterephthalic acid (H_4DOT) and functionalized MWCNTs-COOH (>96%, ID= 6–12 nm, OD= 15–30 nm, length= ~45 µm, Neutrino Co.) were used as purchased without further purification.

2.1. Synthesis of FeCoNi@C-MOF and MWCNTs/FeCoNi@C-MOF powders

FeCoNi-MOF was synthesized via hydrothermal method. Stoichiometric amount of procedure salts ($FeCl_20.4\ H_2O$, $Ni(NO_3)_20.6\ H_2O$, $Co(NO_3)_20.6\ H_2O$) and H_4DOT were dispersed and dissolved in aqueous mixture of distilled water, absolute ethanol and DMF and stirred for 1 h. The stable solution transferred into stainless-steel autoclave and kept at 150 °C for 48 h. The obtained centrifuged powders washed and dried at 70 °C for 24 h in a vacuum oven. Then, for increasing the magnetic features of the MOF powder, it was sintered at 900 °C for 2 h under N2 atmosphere with 5 °C/min heating rate in tube furnace. The final powder is denoted as MOF.

MWCNTs/FeCoNi@C-MOF nanocomposite MWCNTs is synthesized just like as above, using 10 wt% MWCNTs in the first step. the final powder in denoted as M/MOF.

2.2. Characterizations

The X-ray diffraction (XRD) patterns of the powders were characterized with Rigaku D/max-rB, equipped.

with CuK_α radiation. Morphologies observation were carried out with field-emission scanning electron microscopy (FESEM, TESCAN MIRA3 LMU). Magnetic properties were evaluated by vibrating sample magnetometer (VSM, Lakeshore, new 7307 series).

2.3. Electromagnetic measurements

In this study, single and double layer microwave absorbers were made. For single layer microwave absorber each samples were uniformly dispersed in molten paraffin and molded according to X band frequency sample dimension. The filler loading was considered equal to 30 wt% powder and 70 wt% paraffin. The relative complex permittivity and complex permeability were measured by using a vector network analyzer (Agilent N5230A). CST studio suite 2018 using for simulation of microwave absorption performance of double layer absorbers with 2, 2.5 and 3 mm total thickness. In which, X_{min}, X_{max}, Y_{min} and Y_{max} were considered equal to 35 mm with variable Z_{min}, Z_{max}. Boundaries of unit cell were applied in the directions of x and y with using floquet port as wave source with propagation in the direction of z axis. The measured complex permittivity and permeability of single layer MOF and M/MOF are imported as EM parameters in software.

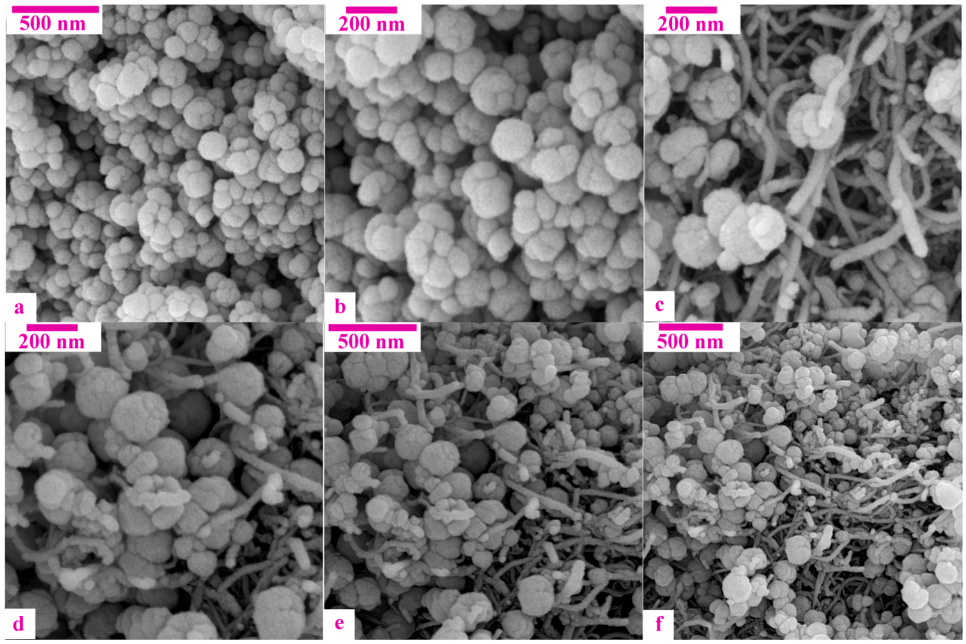

Fig. 2. FESEM images of (a,b) MOF and (c-f) M/MOF samples.

3. Results and discussion

3.1. Structural and morphological analysis

X-ray diffraction analysis was utilized to determine the constituent's phases and structural features of the obtained materials. Fig. 1 indicates the phases present in both MOF and M/MOF samples. It is clearly seen that two sharp and high intensity diffraction peaks centered at 43.8° and 51.0° are related to (111) and (200) facets of FeCoNi alloy which are located exactly between the characteristic diffraction peaks of FeCo and FeNi alloys with 049–1568 and 047–1405 JCPDS, respectively. Besides, no peak related to carbon appears in MOF XRD pattern perhaps due to its amorphous properties. As it can be seen in XRD pattern of M/MOF sample, diffraction peaks at around 26.2°, 44° and 54° can be indexed to (002), (101) and (004) lattice facets of MWCNTs, respectively. Moreover, no impurities were seen in both XRD patterns.

Fig. 2 depicts the FESEM images of as-prepared MOF (Fig. 2a,b) and M/MOF (Fig. 2c-f) samples. As it can be seen, MOF sample show a uniform spheroidal morphology with 100–200 nm diameter. Fig. 2(c-f) shows the mixing condition of the MWCNTs and FeCoNi@C-MOF. It can be concluded from the images that MWCNTs were almost uniformly dispersed and MOF particles were wrapped completely by MWCNTs. Moreover, intermolecular van der Waals forces between the multi walls carbon nanotubes caused entanglement between nanotubes and particles which constructed 3D conductive network that could dedicate excellent microwave absorption capability to the nanocomposite.

3.2. Magnetic characterisation

Magnetic features of MOF and M/MOF samples were evaluated by vibrating sample magnetometer at room temperature. The figure depicts the magnetization versus the external magnetic field curves.

According to the results, S-like hysteresis loops for both MOF and M/MOF samples, confirm soft magnetic materials and ferromagnetic behavior which linked to the presence of ferromagnetic nanoparticles (Fe, Co, Ni) in the composites. The saturation magnetization (M_s) of MOF and M/MOF is 68.77 and 53.15 emu/g respectively. The reduction of M_s value is attributed to the existence of nonmagnetic MWCNTs in the composite and surface spin disorder due to the smaller size of the particles. Moreover, the coercive force (H_c) of the M/MOF increase to 669.7 Oe from 50.59 in MOF sample. Generally, size and composition of the grains, and also crystal orientation are the main factors which affected H_c and M_s of magnetic powder. Accordingly, formation of longitudinal anisotropy due to the growth of particles along the MWCNTs walls are the main reason for increment in H_c of M/MOF. Fig. 3.

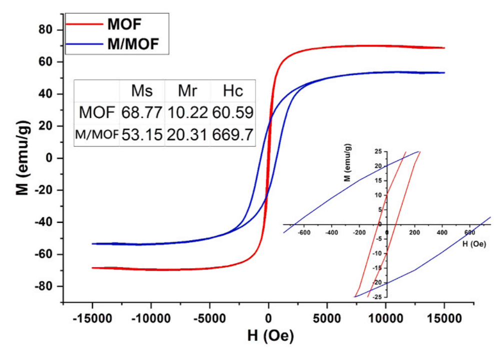

Fig. 3. The hysteresis loops of MOF and M/MOF samples.

3.3. Electromagnetic parameters of MOF and MW/MOF samples

Fig. 4 shows the relative permittivity and the magnetic permeability for MOF and MW/MOF samples.

The addition of MW CNTS clearly induces an increase of dielectric constant and associated dielectric losses. The increase of losses is clearly induced by the conductivity of MWCNTs, while the increase of dielectric constant is ascribed to the Maxwell-Wagner-Sillars polarization effect observed in [2–21] associated to interfacial polarization occurring at the interface between magnetic particles and MWCNTs. The presence of FeNiCo is responsible for a magnetic permeability value higher than 1 in sample MOF. As the saturation magnetization of M/MOF sample is lower than for MOF, so goes it the same for the magnetic permeabilities. The eddy current loss coefficient C_0 and microwave attenuation constant α are expressed by the following equations:

$$C_0 = \mu''\mu'{-}2f^{-1} = 2\pi\mu_0\sigma d^2 \quad (1)$$

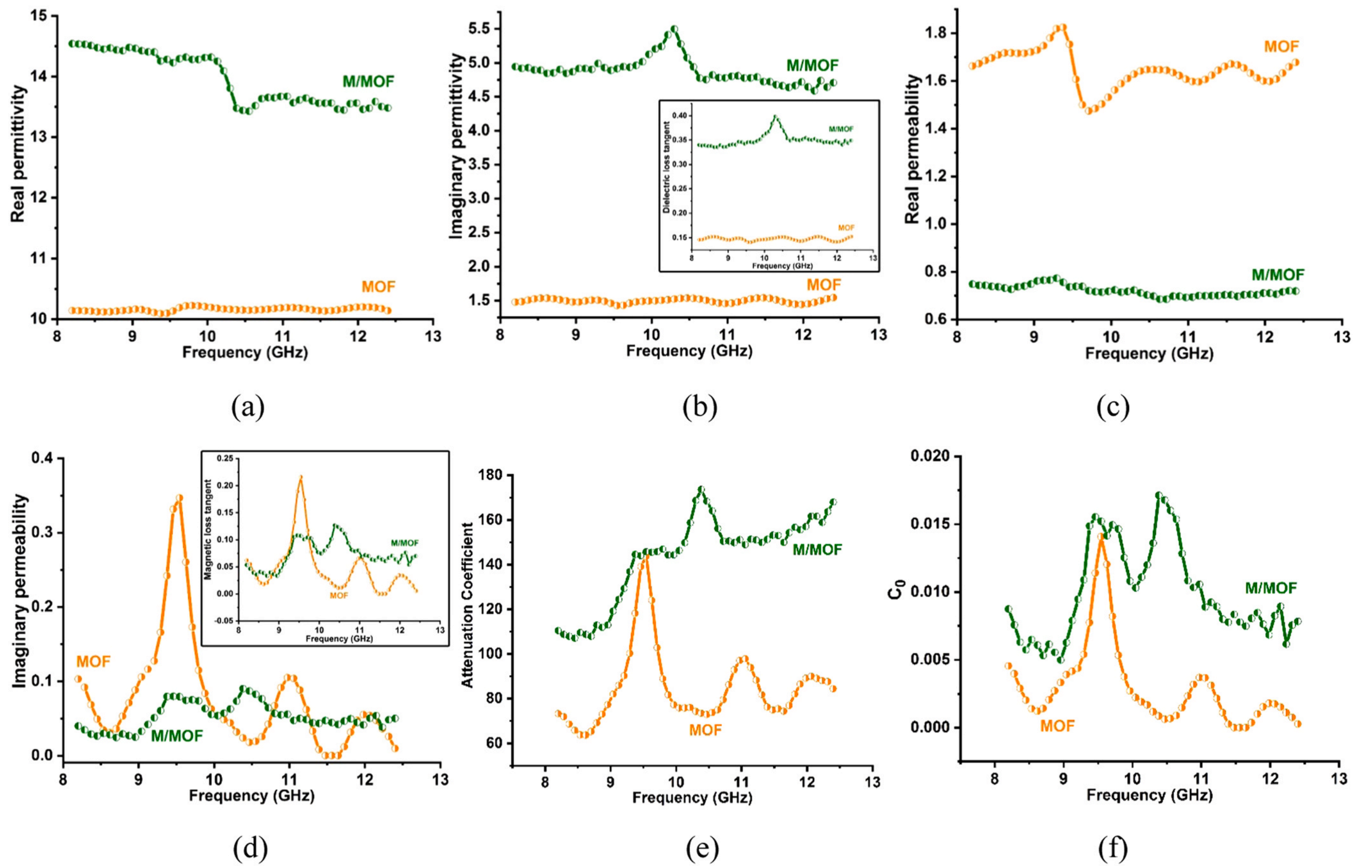

Fig. 4. a-d) Variation of electromagnetic characteristics with frequency, e) attenuation constant and f) C_0 values for MOF and M/MOF samples.

$$\alpha = \frac{2\pi}{c}\sqrt{2\mu'\varepsilon'}\sqrt{\frac{\mu''\varepsilon''}{\mu'\varepsilon'} - 1 + \sqrt{\left(\frac{\mu''}{\mu'}\right)^2 + \left(\frac{\varepsilon''}{\varepsilon'}\right)^2 + \left(\frac{\mu''\varepsilon''}{\mu'\varepsilon'}\right)^2 + 1}} \quad (2)$$

where d, μ_0, and σ represent thickness, permeability in vacuum and electrical conductivity, respectively. As expected from Eq. (2), which shows that α is proportional to ε" and μ", so that the attenuation constant is higher for MMOF/MOF than for MOF sample, this is owing to the respective values shown in Fig. 4(e). As known to all, if the magnetic loss is caused by the eddy current loss mechanism, then C_0 values should be constant by increasing the frequency [22,23]. This is indeed verified in Fig. 4(f).

3.4. Microwave absorption capability

The microwave absorption capability of our samples was also studied via the evaluation of return losses (*RL*) associated to reflection of samples in a Salisbury screen configuration, that is when the absorbing sample is backed by a metallic plate. This configuration mimics the radar operation where signal incident to a target is reflected, allowing its detection by the radar. For stealth applications, *RL* has to be minimized in order to make the target invisible. The Salisbury configuration is adequate to evaluate the absorption capability of a material through the measurement of *RL* since if *RL* is minimized, it means that all signal has been absorbed in the sample so that almost nothing is reflected (nor transmitted since the metallic plate blocks the propagation. *RL* in Salisbury configuration expresses as the reflection coefficient at input interface of an absorber and depends on the input impedance Z_{in} [24]:

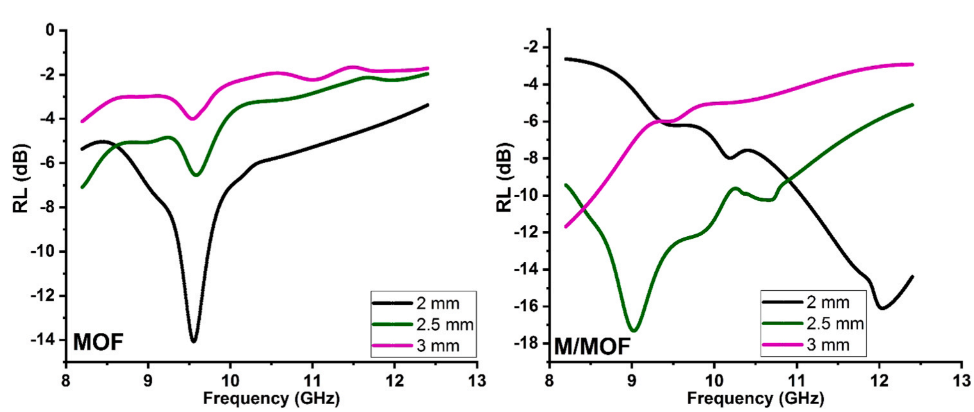

Fig. 5. Reflection loss (RL) of single layer absorber containing MOF (left) and M/MOF (right) with total thickness of 2, 2.5 and 3 mm.

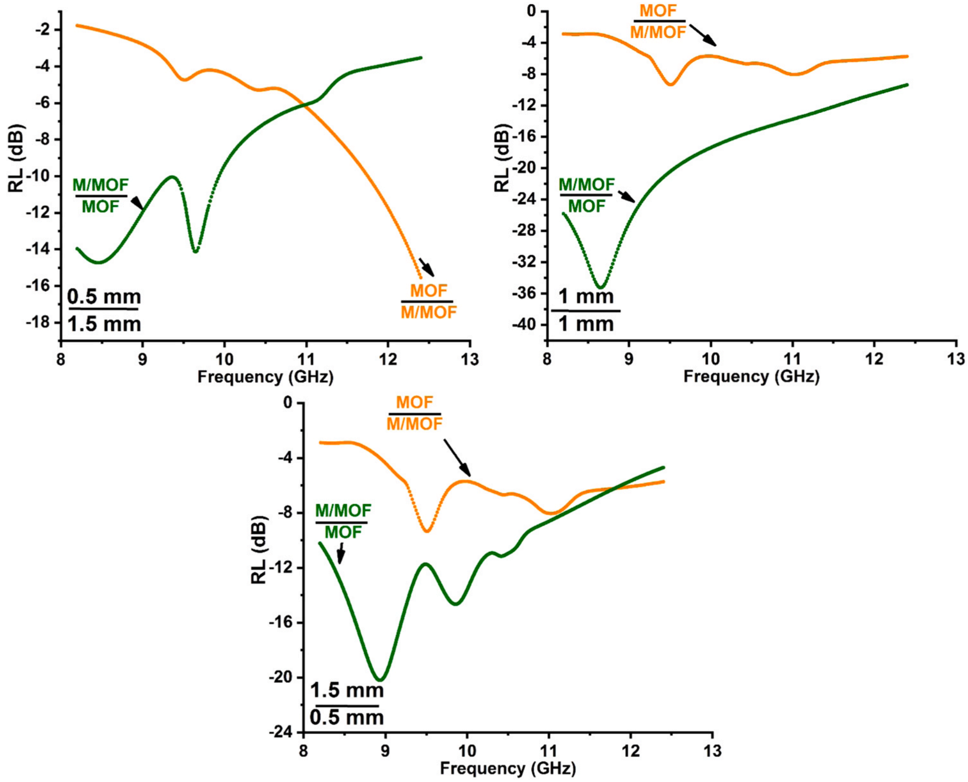

Fig. 6. Reflection loss (RL) of double layer absorber with total thickness of 2 mm.

$$RL = 20\ log_{10}\left(\frac{Z_{in} - Z_O}{Z_{in} + Z_O}\right) \tag{3a}$$

$$Z_{in} = \sqrt{\frac{\mu}{\varepsilon}}\ Z_o\ tanh(\gamma\ d) \tag{3b}$$

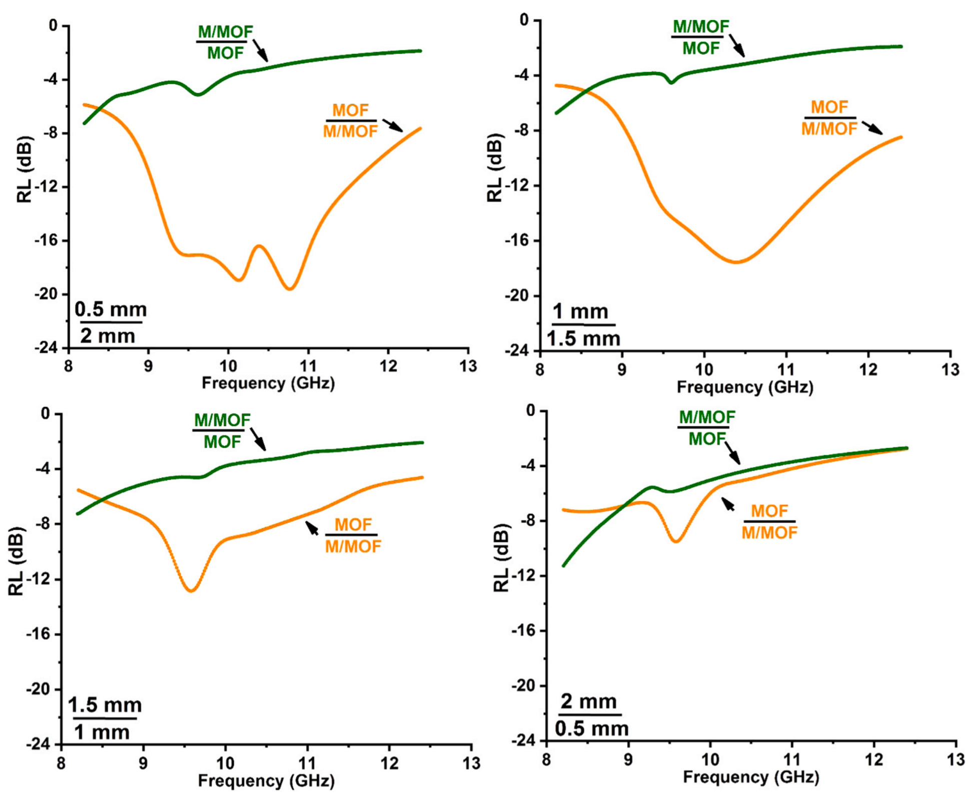

Fig. 7. Reflection loss (RL) of double layer absorber with total thickness of 2.5 mm.

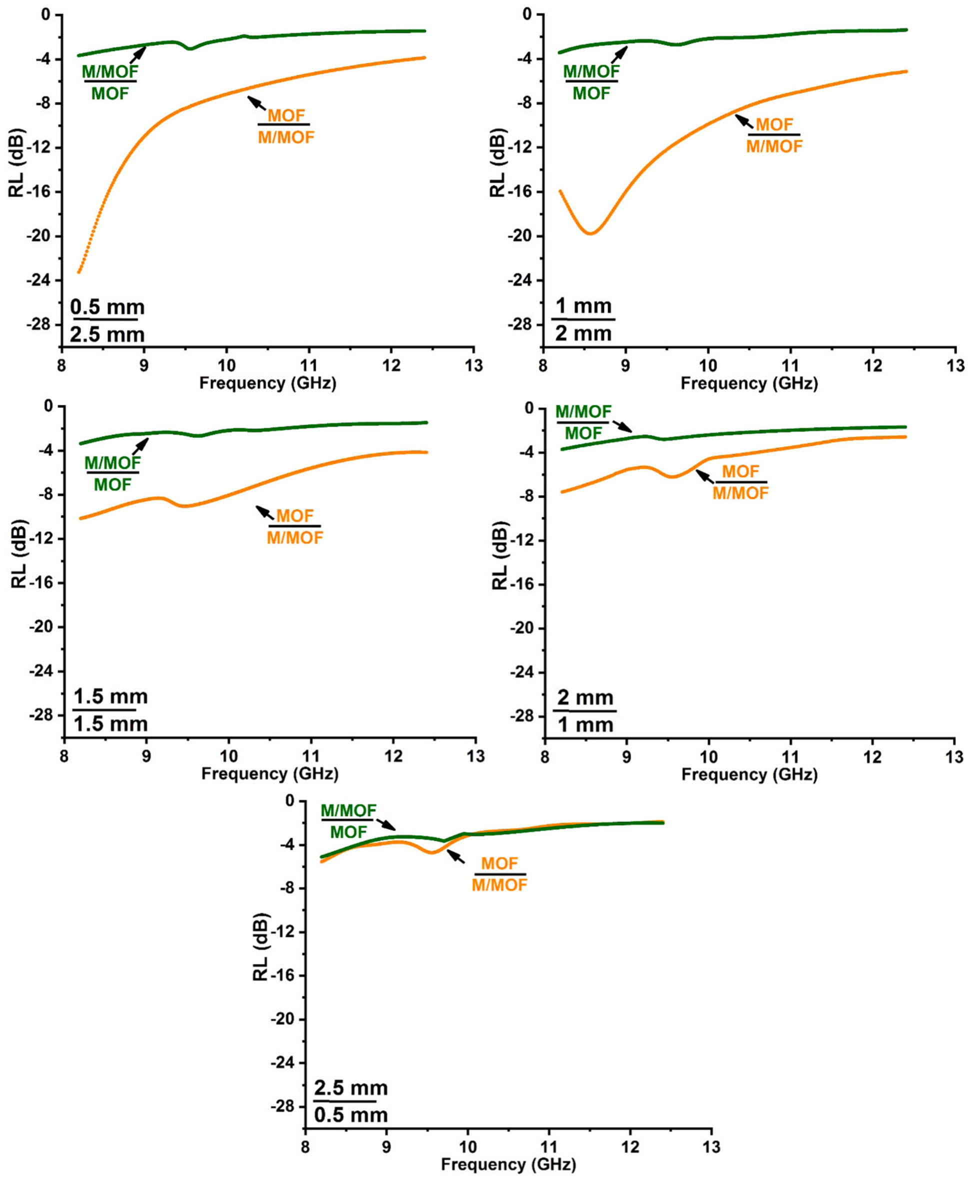

Fig. 8. Reflection loss (RL) of double layer absorber with total thickness of 3 mm.

where

$$\gamma = j2\pi f\sqrt{\varepsilon(1-\tan\delta_\varepsilon)\,\mu\,(1-j\tan\delta_\mu)}\Big/c_O \tag{3c}$$

Z_o is the free-space impedance equal to 377 Ohms, f is the frequency, d is the thickness of the sample and ε_r, μ_r, $\tan\delta_\varepsilon$, $\tan\delta_\mu$ are measured permittivity, permeability and associated loss tangent factors given in Fig. 5, respectively, while c_o is the light velocity in air.

From Eq. (3a) it can be derived that *RL* is minimum, hence the absorption is maximum, when the imaginary part of Z_{in} cancels: this occurs when the thickness *d* of the sample is a multiple of a quarter wavelength λ/4, i.e. at specific frequencies f_o

$$d = n\frac{\lambda}{4} = nC_O\Big/\left(4f\sqrt{\varepsilon\mu}\right)\rightarrow f_O = n\,c_o\Big/\left(d4\sqrt{\varepsilon\mu}\right) \tag{4}$$

3.4.1. Characterization of monolayer absorber

Fig. 5 compares the *RL* values versus frequency at X band for our two samples. It is clear that for sample M/MOF the frequency f_o corresponding to the minimum of *RL* decreases with increasing thickness *d* according to Eq. (2); for sample MOF it moves from 9 GHz to 12.3 GHz when *d* decreases from 2.5 to 2 mm, with *RL* is below −16 d B at those frequencies. For sample MOF the behavior versus thickness is less obvious, since no clear dependence of f_o is observed. In fact for $d = 2$ mm, f_o is around 9.5 GHz, while for higher thicknesses, it moves below 8 GHz, outside the frequency range under scope and thus not visible on the graph. A relevant observation for this sample is that *RL* values are higher than for M/MOF sample, and is well correlated with lower magnetic and dielectric losses observed in Fig. 4, allowing for less absorption.

3.4.2. Characterization of bilayer absorber

Figs. 6, 7 and 8 show the *RL* values simulated for bilayer structures having total thickness of 2, 2.5 and 3 mm respectively. *RL* values for these bilayer absorbers are obtained via simulations using Microwave Studio software, as explained in section 4.4. For each figure, the ratio of thicknesses is varied as well as the order in which the samples are stacked.

MOF/M/MOF means that MOF sample is placed at the input port side, and is followed by M/MOF sample backed by the metal plate. Reversely, M/MOF/MOF means that M/MOF sample is at the input and is followed by MOF sample backed by the metal.

Table 1
Comparison of absorption performances of samples.

Sample	thickness (mm)	Fo (GHz)	BW (GHz)	|RL| (dB)	FB (%)	FOM
MOF	2	9.6	0.4	14	4.2	58
MMOF	2	12.1	2	16	16	256
MMOF	2.5	9.2	2	18	22	396
MMOF	3	8	0.4	12	5	60
MMOF/ MOF	0 0.5 + 1.5	8.5	2	15	23	345
MMOF/ MOF	1 + 1	8.7	**5**	**36**	**57**	**2052**
MMOF/ MOF	1.5 + 0.5	9	**3**	**22**	**33**	**726**
MOF/ MMOF	0.5 + 2	10.5	**3**	**20**	**28**	**560**
MOF/ MMOF	1 + 2.5	10.5	**3**	**18**	**28**	**504**
MOF/ MMOF	2.+ 0.5	9.8	0.4	14	4	56
MOF/ MMOF	1 + 2	8	1.5	24	18	432
MOF/ MMOF	1.5 + 1.5	8.7	**2.5**	**20**	**28**	**560**

For 2 mm, Fig. 6, it is clear that *RL* of the stack M/MOF / MOF is much better than for stack MOF / M/MOF. For each stack, the minimum of *RL* occurs around 8–9 GHz, which corresponds to the frequency where the thickness is equal to the quarter wavelength calculated with averaged values over thickness of permittivity and permeability extracted from Fig. 4. Moreover, *RL* decreases with in increasing thickness of M/MOF layer, well correlated with higher losses content associated with of M/MOF material inducing higher absorption.

For thickness *d* equal to 2.5 mm, Fig. 7, the situation seems inverted, since the stack MOF/MMOF shows much lower RL values than for stack M/MOF / MOF. Minimum occurs around 10–10.5 GHz and bandwidth of absorptions seems much larger.

Finally for $d = 3$ mm, Fig. 8, *RL* remains higher than −12 dB for all M/MOF/MOF stack configurations and for the two MOF/ M/MOF configurations having the highest thickness of MOF layer. This is explained by the fact that the thickness is too high for inducing resonance at X band, so that it will occur below 8 GHz, and no minimum of *RL* is present in the X band. For the two MOF and M/MOF samples having the lowest MOF thickness, minimum of RL appears around 8 GHz. Indeed, the main contribution comes from the M/MOF sample, for which resonances in the X band are possible, as seen in Fig. 5.

3.4.3. *Comparison of performances*

The following Table 1 enables a more quantitative comparison between performances of mono- and bilayer structures. In view of this the following definitions are proposed:

- the −10 dB bandwidth, noted BW and defined as the frequency range where RL ≤ 10 dB
- the fractional bandwidth defined as $FB = W/f_o$, where f_o is the center frequency of the absorption bandwidth BW
- the figure of merit defined as FOM = FB x |RL|; this figure indicates that we are interested in having the highest magnitude of reflection losses |RL| over the highest possible frequency range.

A good absorber classically satisfies RL ≤ 10 d B. Samples from Figs. 5 to 8 that are not satisfying this criterion are excluded from the table.

From Table 1 it can be concluded that five samples, marked in bold face, stand out in term of FOM. They all belong to the bilayer category. Their superiority results from the fact that both FB and |RL| are higher than for the other samples.

This observation demonstrates that bilayer configurations increase the FOM, by maximizing the bandwidth and minimizing the return loss responsible for absorption in the material.

The better absorption performance of the double-layer absorber maybe attributed to the better impedance matching ability of M/MOF layer, coupling interactions between two distinctive layers (absorbing and matching layers) and excellent magnetic loss ability of MOF layer.

The absorber operating in Salisbury configuration exploits a resonant behavior occurring when the thickness *d* of the sample is a multiple of the operating quarter wavelength as given by Eq. (4); at the corresponding frequency the reflected signal returns to the input of the absorber with a 180° phase shift while being almost totally attenuated by absorption induced by in the lossy material characterized by the attenuation constant $\alpha = Re\,(\gamma)$ from (2) shown in Fig. 4(e), so that Z_{in} becomes a real number proportional to the losses in the material. As expected it increases in presence of CNT included in MMOF type samples, as following dielectric losses shown in Fig. 4. The higher the losses in the material, the more Z_{in} is close to Z_o, minimizing thus *RL* by virtue of Eq. (3a). Fig. 9(a) shows the behavior of Z_{in} as a function of frequency for the double layer configuration of Fig. 7 right, having a thickness 1 + 1.5 mm. For sample MOF/MMOF the imaginary part of Z_{in} cancels at 10 GHz, while its real part becomes close to Z_o, so that matching occurs and a minimum of *RL* is achieved, as shown in Fig. 7 right. A contrario for sample MMOF/MOF the imaginary part of impedance never cancels in the 8–14 frequency range, and the real part is too low, so that matching cannot appear for MMOF/MOF configuration in Fig. 7 right. Matching occurs below 8 GHz, around 7 GHz, not visible in the range of Fig. 7 right. For comparison Fig. 9(b) shows the behavior of monolayers having the same thickness equal to 2.5 mm. At the resonant frequency, 8 GHz for MOF sample and 9.8 GHz for MMOF/MOF samples, the real part of impedance is respectively to high or too low to induce matching. Thus Fig. 9 demonstrates the superiority of double-layer over single layer configuration.

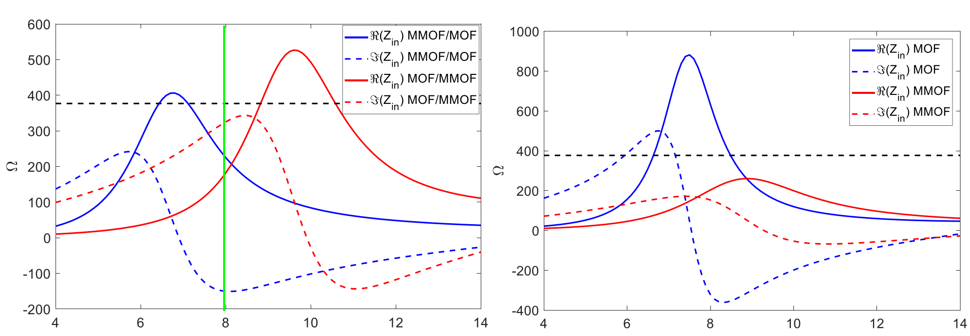

(a) (b)

Fig. 9. Input impedance Z_{in} for (a) double layer having thickness 1 + 1.5 mm as in Fig. 7 (right) (b) single layer having thickness 2.5 mm.

4. Conclusion

In this paper FeCoNi@C metal−organic framework (MOF) and MWCNTs decorated with MOF (MW/MOF) were successfully synthesized via hydrothermal method and characterized with XRD, VSM and FESEM.

MOF sample shows a uniform spheroidal morphology with 100–200 nm diameter, while for M/MOF sample images show that MWCNTs are almost uniformly dispersed and MOF particles were wrapped completely by MWCNTs.

VSM measurements reveal S-like hysteresis loops for both MOF and M/MOF samples, confirming soft magnetic materials and ferromagnetic behavior which linked to the presence of ferromagnetic nanoparticles (Fe, Co, Ni) in the composites.

Measurements of electromagnetic parameters, dielectric permittivity, magnetic permeability and associated losses, are used to predict by simulations the return losses for bilayer configurations including various combinations of thickness and stacking order. It is concluded from the exhaustive comparison using a FOM gauge that five combinations of thickness and stacking order achieve FOM values higher than 500, meaning a large absorption over a wide frequency range. These five samples belong to the bilayer category, which demonstrates the relevance of these structures.

Funding

The research of Isabelle Huynen as Research Director is funded by the National Fund for Scientific Research (FNRS), Belgium.

Author statement

The authors warrant that the article is the *authors*' original work, hasn't received prior publication and isn't under consideration for publication elsewhere.

Declaration of Competing Interest

The authors declare that they have no known competing financial interests or personal relationships that could have appeared to influence the work reported in this paper.

References

[1] N. Violette, Electromagnetic Compatibility Handbook, Springer, Berlin/Heidelberg, Germany, 2013.
[2] A. Saib, L. Bednarz, R. Daussin, C. Bailly, X. Lou, J.-M. Thomassin, C. Pagnoulle, C. Detrembleur, R. Jerome, I. Huynen, Carbon nanotube composites for broadband microwave absorbing materials, IEEE Trans. Microw. Theory Tech. 54 (2006) 2745–2754.
[3] B. Chambers, Optimum design of a Salisbury screen radar absorber, IEE Electron. Lett. 30 (1994) 1353–1354.
[4] J.-B. Kim, Design of Salisbury screen absorbers using dielectric lossy sheets. In Proceedings of the 2011 IEEE International Conference on Microwave Technology & Computational Electromagnetics, Beijing, China, 22–25 May 2011; pp. 1–2.
[5] J.-H. Oh, Oh Kim C.-G., C.-S. Hong, Design of radar absorbing structures using glass/epoxy composite containing carbon black in X-band frequency ranges, Compos. Part B 35 (2004) 49–56.
[6] J.-B. Kim, S.-W. Lee, C.-G. Kim, Comparison study on the effect of carbon nano materials for single-layer microwave absorbers in X-band, Compos. Sci. Technol. 68 (2008) 2909–2916.
[7] B. Kim, Broadband radar absorbing structures of carbon nanocomposites, Adv. Compos. Mater. 21 (2012) 333–344.
[8] P.M. Raj, D. Mishra, D., H. Sharma, S. Swaminathan, R. Tummala, Chap. 1 Nanomagnetic materials and structures, and their applications in integrated rf and power modules, Nanomagnetism (2014) 1–29.
[9] F. Qin, H.X. Peng, H.X. Pankratov N.Y., M. Phan, L.V. Panina, M. Ipatov, V. Zhukova, A. Zhukov, J. Gonzalez, Exceptional electromagnetic interference shielding properties of ferromagnetic microwires enabled polymer composites, J. Appl. Phys. 108 (2010), 044510.
[10] X. Ma, Q. Zhang, Q.Z. Luo, X. Lin, G. Wu, A novel structure of ferroaluminum-based sandwich composite for magnetic and electromagnetic interference shielding, Mater. Des. 89 (2016) 71–77.
[11] K. Singh, A. Ohlan, A. Bakhshi, S. Dhawan, Synthesis of conducting ferromagnetic nanocomposite with improved microwave absorption properties, Mater. Chem. Phys. 119 (2010) 201–207.
[12] X. Liang, B. Quan, G. Ji, W. Liu, H. Zhao, S. Dai, J. Lv, Y. Du, Tunable dielectric performance derived from the metal−organic framework/reduced graphene oxide hybrid with broadband absorption, ACS Sustain. Chem. Eng. 5 (2017) 10570–10579.
[13] K. Zhang, F. Wu, Y. Jiao, M. Sun, Y. Xia, A. Xie, The synthesis of core–shell nanowires with intense dielectric and magnetic resonance properties at microwave frequency, J. Mater. Chem. C 7 (2019) 3590–3597.
[14] X.J. Zhang, G.S. Wang, W.Q. Cao, Y.Z. Wei, J.F. Liang, L. Guo, M.S. Cao, Enhanced microwave absorption property of reduced graphene oxide (RGO)-MnFe2O4 nanocomposites and polyvinylidene fluoride, ACS Appl. Mater. Interfaces 6 (2014) 7471–7478.
[15] Y. Jiao, J. Li, A. Xie, F. Wu, K. Zhang, W. Dong, X. Zhua, Confined polymerization strategy to construct polypyrrole/zeolitic imidazolate frameworks (PPy/ZIFs) nanocomposites for tunable electrical conductivity and excellent electromagnetic absorption, Compos. Sci. Technol. 174 (2019) 232–240.
[16] X. Sun, X. Lv, M. Sui, X. Weng, X. Li, J. Wang, Decorating MOF-derived nanoporous Co/C in chain-like polypyrrole (PPy) Aerogel: a lightweight material with excellent electromagnetic absorption, Materials 11 (2018) 781.
[17] A.L. De Paula, M.C. Rezende, J.J. Barroso, Experimental measurements and numerical simulation of permittivity and permeability of Teflon in X band, J. Aerosp. Technol. Manag. 3 (2011) 59–64.
[18] D. Xu, M. Jafarian, S. Afghahi, A. Atassi, A.M. Bani, A.O. Rama, Remarkable microwave absorption efficiency of low loading ratio of Ni0.25Co0.25Ti0.5Fe2O4/SrCoTiFe10O19/Cu composite coated with polyprrole within polyurethane matrix, Mater. Res. Express 7 (2020), 016103.
[19] G. Cui, Y. Lu, W. Zhou, X. Lv, J. Hu, G. Zhang, G.; G. Gu, Excellent microwave absorption properties derived from the synthesis of hollow Fe3o4@reduced graphite oxide (RGO) nanocomposites, Nanomaterials 9 (2019) 141.
[20] R. Jaiswar, C. Bailly, S. Hermans, J.P. Raskin, I. Huynen, Wideband microwave absorption in thin nanocomposite films induced by a concentration gradient of mixed carbonaceous nanostructures, J. Mater. Sci. Mater. Electron. 30 (2019) 19147–19153.
[21] A. Emplit, I. Huynen, Study of absorption in carbon nanotube composites from 1HZ to 40GHZ, Int. J. Microw. Eng. 2 (2017) 01–13.
[22] X.J. Zhang, G.S. Wang, W.Q. Cao, Y.Z. Wei, J.F. Liang, L. Guo, M.S. Cao, Enhanced microwave absorption property of reduced graphene oxide (RGO)-MnFe2O4 nanocomposites and polyvinylidene fluoride, ACS Appl. Mater. Interfaces 6 (2014) 7471–7478.
[23] G. Cui, Y. Lu, W. Zhou, X. Lv, J. Hu, G. Zhang, G. Gu, Excellent microwave absorption properties derived from the synthesis of hollow Fe3o4@reduced graphite oxide (RGO) nanocomposites, Nanomaterials 9 (2019) 141.
[24] D. Pozar, In Microwave Engineering, second ed,, Wiley, New York, USA, 1998.